JOURNAL OF CATALYSIS 157, 501–511 (1995)

Synthesis, Characterization, and Catalytic Properties of Micro-Mesoporous, Amorphous Titanosilicate Catalysts

A. Keshavaraja, Veda Ramaswamy, H. S. Soni, A. V. Ramaswamy, and P. Ratnasamy

National Chemical Laboratory, Pune 411 008, India

Received October 3, 1994; revised May 10, 1995; accepted July 26, 1995

Titanosilicates, synthesized under ambient conditions in the absence of nitrogenated organic bases, exhibit (i) an amorphous nature (XRD, electron diffraction, TEM); (ii) a bimodal, narrow pore size distribution with pore widths around 0.8 and 3.6 nm, respectively, and surface areas of about 500–700 m^2g^{-1} (BET); (iii) absorption bands at 960 cm^{-1} (IR) and 220 nm (UV), respectively; (iv) a radial electron density distribution pattern indicating the presence of isolated TiO_4 units in a silica matrix; and (v) catalytic activity and selectivity comparable to crystalline TS-1 (MFI) in the oxidation (with aqueous H_2O_2) of benzene, toluene, and phenol. Unlike other solid catalysts known so far, these amorphous titanosilicates provide a higher yield of catechol than hydroquinone in the oxidation of phenol. In contrast to TS-1 or TS-2 (MEL), the oxyfunctionalization of the side chain in toluene is more predominant than the aromatic ring hydroxylation indicating a radical mechanism of oxidation. © 1995 Academic Press, Inc.

INTRODUCTION

The introduction of aluminosilicate zeolites as catalysts in the early sixties had a significant impact on industrial catalysis. Since then, small pore (erionite), medium pore (ZSM-5), and large pore (faujasites, mordenite, zeolite-L and beta) zeolites have been used extensively for various (mainly acid-catalyzed) chemical transformations. The advent of titanosilicate molecular sieve, TS-1, with MFI structure in the early eighties represented the next major innovation enabling shape-selective oxidations to be carried out on an industrial scale (1). Subsequently, other titanosilicate molecular sieves like TS-2 (MEL) (2), TS-48 (the titanium analog of ZSM-48) (3), and TS-beta (titano–aluminosilicate analog of zeolite beta) (4) have all been synthesized, broadening the scope of oxidation catalysis with molecular sieves. All the above-mentioned materials are microporous with an average pore radius less than 1.0 nm, thereby imposing a constraint on the size of the organic substrate that can be oxyfunctionalized. Very recently, Tanev *et al.* (5) announced the synthesis of titanium-containing hexagonal mesoporous silica (Ti–HMS) with a pore diameter of around 2.8 nm and significant catalytic activity in the oxidation of bulky molecules like 2,6-di*tert*-butyl phenol. Almost simultaneously, Corma *et al.* (6) and Franke *et al.* (7) reported the preparation and properties of Ti-containing MCM-41. The oxidation of alpha terpineol and norbornene using *tert*-butyl hydroperoxide as the oxidant is reported by Corma *et al.* (6). One common characteristic of all the titanosilicate molecular sieves mentioned above, including Ti–HMS, is that they are all crystalline materials prepared in the presence of nitrogenated organic bases. Recently, Toba *et al.* (8) have compared different methods of preparation of titania–silicas (Si/Ti = 0.5–25) and concluded that those prepared using diols as complexing agents are more homogeneous and have better Ti–O–Si bond formation. Their catalytic activity was not reported.

In the present study, we report the synthesis of micro-mesoporous amorphous titanosilicates (designated as MMATS) in the *absence* of nitrogenated organic bases. These materials are able to oxyfunctionalize organic molecules using aqueous H_2O_2 as oxidant with an activity and selectivity somewhat similar to TS-1. MMATS have been additionally characterized by X-ray diffraction/scattering, ESCA, IR/UV–Vis/Raman spectroscopies, SEM, TG/DTA, TPR (H_2), ^{29}Si MAS NMR, and sorption (Ar, H_2O, benzene, cyclohexane, 1,3,5-tri-isopropyl benzene) techniques.

EXPERIMENTAL

Preparation

MMATS were prepared by a modified sol–gel method. Typically, 1 mol of tetraethyl orthosilicate (TEOS) (Aldrich, 99%) in ethanol was slowly added to 0.06 mol of titanium butoxide (Aldrich, 99%) in 2-propanol at 313 K and neutral pH over a period of 6 h. Deionized water mixed with 2-propanol was then added to the above mixture in a controlled manner (0.1 ml per min) to produce a clear, transparent gel. The material was aged for 24 h at 313 K and then H_2O and alcohol were removed by vacuum

0021-9517/95 $12.00

treatment. The resultant semi-dry gel was further dried at 383 K for 24 h under vacuum and then calcined in air at 723 K for 24 h. Three such samples with Si/Ti ratios of 17, 34, and 51 (designated as samples A, B, and C, respectively) were prepared. A Ti-free silica was also prepared from TEOS in a similar way. We have also prepared, for comparison, a microporous, crystalline titanosilicate (TS-1) with MFI structure using tetrapropylammonium hydroxide as organic base using a procedure described elsewhere (9). The samples were chemically analyzed by atomic absorption spectroscopy (Hitachi).

Characterization

The X-ray scattering measurements were made with Cu$K\alpha$ radiation on a computer-controlled XRD (Rigaku, D-Max/III VC model) instrument, equipped with a reflection geometry, a NaI scintillation counter, a curved graphite crystal monochromator, and a nickel filter. The scattered intensities were collected from 3.5° to 130° (2θ) by scanning at 0.5° (2θ) steps with a counting time of 15 s at each step. The sample was rotated throughout the scanning period. The intensities were corrected for air scattering, polarization, and absorption effects and then normalized to convert the corrected intensities to electron units. Using the theoretical values of the Compton scattering intensities of silicon, titanium, and oxygen as a function of $\sin\theta/\lambda$, the normalized radial distribution function was computed (10).

The framework IR spectra of the samples were recorded in a Nicolet (60 SXB model) FTIR instrument, after deposition of the sample as a thin film on a Si plate and subsequent removal of the background vibration due to Si. The laser Raman (Spex 1403 spectrometer, Ar ion laser) spectra of self-supported, thin pellet of the samples were recorded after evacuation of the sample to 10^{-3} Torr (1 Torr = 133 Pa). The ^{29}Si MAS NMR (Bruker, MSL-300) spectra of the samples were recorded at 59.6 MHz and referenced to Me_4Si. The XPS measurements were carried out in a VG Scientific ESCA-3 MK2 electron spectrometer with an Al$K\alpha$ X-ray source. A binding energy of 285 eV for the C 1s level was used as internal standard. The sorption measurements were carried out gravimetrically in a (Cahn, 2000 G) electrobalance at 298 K and at a fixed p/p_0 of 0.5 after equilibration for 10 h. The samples were evacuated at 673 K to 10^{-6} Torr for 6 h before adsorption measurements. The surface areas (BET), the micropore and mesopore volume, and the pore size distributions were calculated from the Ar adsorption/desorption isotherms at liquid N_2 temperature in a Coulter (Omnisorb 100 CX) instrument. The micropore size distributions were calculated from the low pressure region ($p/p_0 = 10^{-4}$ to 0.1) of the isotherms following the Horvath and Kawazoe model (11) and the mesopore distribution from the desorption isotherms using the BJH model (12).

Scanning electron micrographs were taken in a Jeol (model 5200) instrument. TEM and electron diffraction of the sample were carried out in a Jeol (model 1200 EX) electron microscope. Simultaneous TG and DTA of the samples were performed in a TG/DTA-92 model (Setaram, France) instrument under air flow at 100 cm^3 min^{-1} with a heating rate of 10 K min^{-1} up to 1270 K. Temperature-programmed reduction of the samples was carried out in a Sorbstar (Hungary) instrument using 5 vol% H_2–N_2 mixture at a heating rate of 18 K min^{-1}.

Catalytic Activity

The hydroxylation and oxidation reactions were carried out in a batch reactor using benzene, phenol, and toluene as organic substrates and aqueous H_2O_2 (26 wt%) as the oxidant. Invariably, a substrate to catalyst (wt) ratio of 10 and a substrate to H_2O_2 (mol) ratio of 3 were employed with either acetone, water, or acetonitrile as solvent. Other details of the reaction and of product analysis are given elsewhere (13).

RESULTS AND DISCUSSION

Characterization

X-ray, electron diffraction, and TEM. The X-ray diffraction patterns of these samples did not contain any sharp reflections but only a broad diffuse band similar to that of amorphous silica. In particular, no separate crystalline phase of TiO_2 (like anatase) could be detected. These materials are, hence, completely amorphous without any long-range order. Even samples calcined above 1073 K did not show the formation of a separate anatase or a rutile phase and there was no indication of the crystallization of either the silica or titania on such thermal treatment. An electron diffraction analysis of sample A showed only a halo pattern and its TEM image did not indicate the presence of any crystalline TiO_2. However, this does not necessarily mean that regions with short range order similar to that in crystalline TiO_2 are absent in our samples. Imamura *et al.* (14) and Saito (15) have argued that very fine crystalline particles could be present even in samples which are apparently amorphous to XRD, electron diffraction, and TEM imaging.

ESCA. The bulk chemical composition (from wet chemical analysis) and surface composition (from ESCA) in terms of Si/Ti ratios of the three samples (A–C) are given in Table 1. There is an apparent surface enrichment of Si. Surface depletion of TiO_2 has been observed in many titania–silica systems (14) including TS-1 (Table 1) and Ti glasses (16). A plausible explanation is that occupancy by Ti is energetically less favored than occupancy by Si on the surface where the silica network is disrupted (14, 16). Figure 1 shows the Ti2p photoelectron peaks of samples

TABLE 1

Physicochemical Properties of MMATS Samples A–C, SiO_2, TiO_2, and TS-1

Sample	Si/Ti ratio (mol)		B.E. (eV) (ESCA)		Surface area (m^2/g)			Pore volume (ml/g)			Av. pore widths (nm)	
	Bulk	Surface	Si $2p_{1/2}$	Ti $2p_{3/2}$	Micro	Meso	Total	Micro	Meso	Total	Micro	Meso
A	17	32	103.6	459.5	462	162	624	0.22	0.11	0.33	0.85	3.6
B	34	53	103.6	459.6	478	105	583	0.21	0.09	0.30	0.86	3.6
C	51	81	103.6	459.8	506	46	552	0.22	0.04	0.26	0.85	3.6
SiO_2	—	—	104.0	—	563	31	594	0.22	0.02	0.24	0.75	—
TiO_2	—	—	—	458.9	—	47	47	—	0.22	0.22	—	18.8
TS-1	32	125	103.9	460.5	400	15	415	0.18	—	0.18	0.58	—

A–C in comparison with those of pure TiO_2 and TS-1. Compensation for work function shifts due to specimen charging has been made. The ESCA binding energies of Si and Ti (Table 1) are those expected for Si^{4+} and Ti^{4+} ions, respectively. The actual peak separation for TS-1 is smaller (4.7 eV) compared to that of the MMATS samples (5.2 to 6.4 eV). For pure TiO_2, the Ti $2p_{3/2}$ binding energy value is 458.9 eV. There is a small but significant increase in the binding energy of Ti $2p_{3/2}$ electrons in samples A, B, and C (459.5, 459.6, and 459.8 eV, respectively), while that of Si $2p_{1/2}$ decreases marginally. These trends are similar to those observed by Imamura *et al.* (14) for their titania–silica samples and indicate the formation of Si–O–Ti species through an interaction between Ti and Si atoms. The difference in binding energies has been attributed to fourfold coordination with oxygen (of Ti) in Ti silicate glasses (16, 17). The binding energy shift is more prominent in TS-1 (1.6 eV).

The O 1*s* spectra of the samples shown in Fig. 2 provide further evidence for the formation of Si–O–Ti linkages. The symmetrical O 1*s* peaks of pure SiO_2 and pure TiO_2 appear at 533.5 and 530.2 eV, respectively, whereas the samples A, B, and C show asymmetry due to the presence of a minor Si–O–Ti component and a major Si–O–Si component. The core electron binding energy of the oxygen atom is decreased when a Si–O–Si bond is replaced by Ti–O–Si. The O 1*s* peaks in Ti-doped silica are wider than those of pure silica. The FWHM of this peak varies linearly with increasing Ti content (2.5, 2.7, and 3.1 eV, respectively). These observations are similar to those reported for amorphous titania–silica glasses (17–19).

Adsorption. Some of the textural properties of these samples are given in Table 1. The Ar adsorption–desorption isotherm of one of the samples is shown in Fig. 3 (inset) along with those of silica and titania prepared in a similar manner. Three stages can be observed in the plot for the MMATS sample; a sharp linear increase going through the origin at very low partial pressures of Ar due to monolayer–multilayer adsorption in micropores, a more gradual increase at higher partial pressures of Ar indicative of multilayer adsorption in mesopores, and finally a capillary condensation above $p/p_0 = 0.4$. The mesopore area (from the *t*-plot) and the total surface area (BET) values are also given in Table 1. It is seen that as the Ti content increases, the surface area of mesopores increases significantly. A corresponding increase in mesopore volume is also noticed on increasing the Ti content. In fact, the increase in pore volume due to Ti incorporation is due entirely to the generation of mesopores (Table 1). The pore-width of the micro- and mesopores were calculated to be around 0.85 and 3.6 nm, from Horvath–Kawazoe and the BJH plots (Fig. 3), respectively. These materials, hence, possess a bimodal and a fairly narrow pore size distribution. In general, when a material is prepared by sol–gel method under basic pH, the rate of hydrolysis is faster than the rate of condensation and the resulting material is essentially mesoporous. Under mildly acidic conditions, the rate of condensation is faster than the rate of hydrolysis and one would get microporous material. We have maintained almost neutral pH in our preparation which probably led to a bimodal pore size distribution in the samples. In addition, we have observed that the rates of hydrolysis and condensation of TEOS is influenced by the presence of even small concentrations of Ti alkoxides.

A major part of the surface area is contributed by pores with a diameter characteristic of micropores (less than 2.0 nm). A smaller but significant part is due to mesopores with pore diameters between 2.0 and 20 nm (Table 1). The Ti-free silica prepared from TEOS is found to be essentially microporous whereas pure TiO_2 (anatase) has a low surface area, due to the presence of mesopores with a broad pore size distribution. The MMATS samples lose their surface areas on calcination above 923 K (Fig. 4) due to the loss of micropores.

The sorption capacity of MMATS samples and of pure SiO_2 for H_2O and some hydrocarbons is summarized in

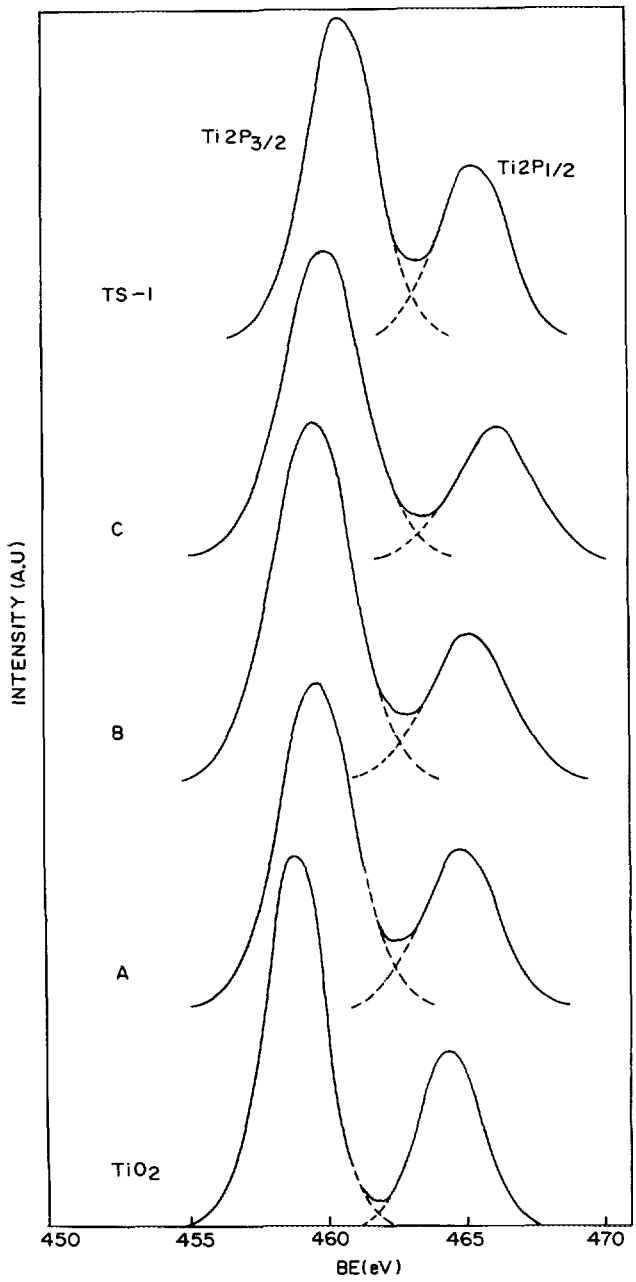

FIG. 1. Ti 2*p* photoelectron spectra of TiO_2, MMATS samples A to C, and titanium silicalite, TS-1.

Table 2. For all the adsorbates including the bulkier 1,3,5-trimethyl- and tri-isopropylbenzenes, the amount adsorbed under the conditions given in Table 2 is significant and increases with the Ti content in the sample in parallel with the increase in the mesopore volume and the surface area of the samples (Table 1). In the absence of values for the other mesoporous titanium silicates known so far, viz., Ti–MCM-41 and Ti–HMS (5, 6), it is difficult to compare the relative adsorption capacities of all three of these materials. It can be seen from Table 2 that the sorption capacity of pure silica, which is essentially microporous, is relatively less than that of the MMATS samples.

Scanning electron microscopy. The scanning electron micrographs of samples A–C are shown in Fig. 5. The average particle size is between 0.2 and 0.5 μm. As expected for amorphous materials, they are irregular in shape but fairly uniform in size.

Thermal analysis. The TG/DTA thermograms of samples A–C (Fig. 6) reveal only the endothermic loss of water in the temperature range, 273–500 K. No exotherm due to crystallization and segregation of a TiO_2 phase is seen

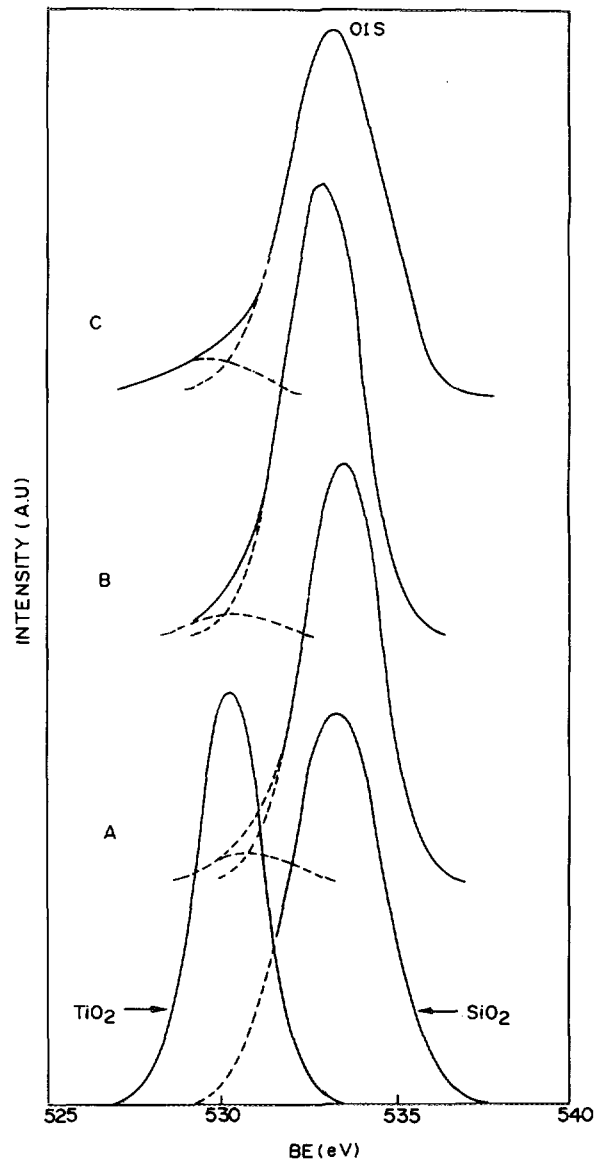

FIG. 2. O 1*s* photoelectron spectra of TiO_2, SiO_2, and MMATS samples A to C.

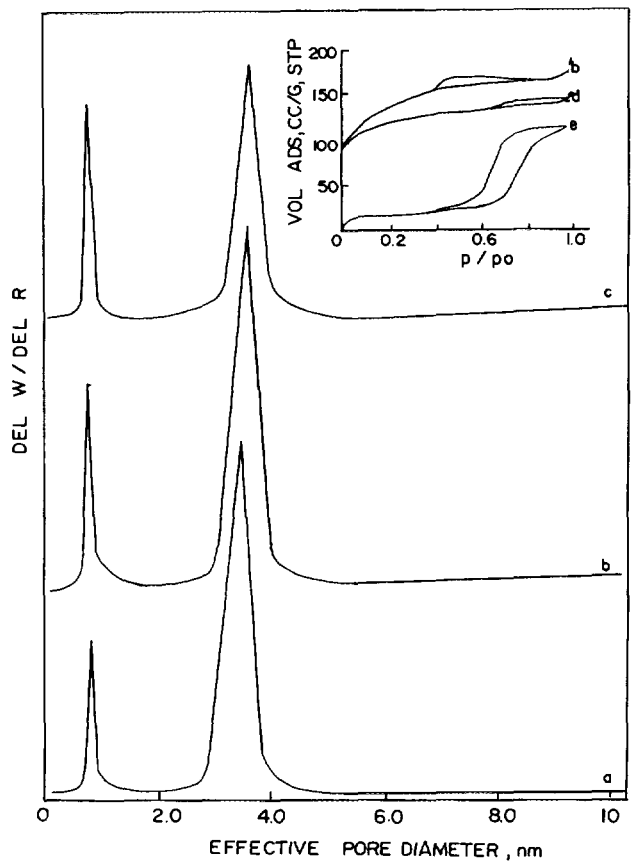

FIG. 3. Pore size distribution in MMATS samples A to C (curves a to c, respectively). Inset: Ar adsorption–desorption isotherms at 77 K, of sample B (curve b), pure SiO_2 (curve d), and pure TiO_2 (curve e).

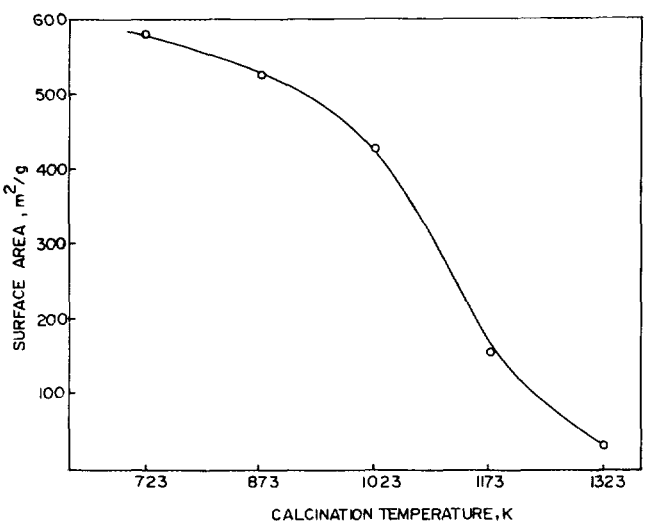

FIG. 4. Influence of calcination temperature on the surface area (BET) of MMATS-B sample (Si/Ti = 34).

TABLE 2

Sorption Capacity of MMATS Samples (wt%)[a]

Adsorbate	Samples			
	A	B	C	SiO_2
Water	25.1	21.0	21.9	17.6
n-Hexane	16.8	14.2	11.3	9.7
Cyclohexane	19.3	14.1	10.0	8.4
Benzene	26.0	19.5	16.7	13.7
1,3,5-trimethyl benzene	23.0	18.2	14.6	9.7
1,3,5-tri-isopropyl benzene	18.8	15.0	11.4	1.3

[a] Gravimetric adsorption in Cahn Electrobalance at $p/p_0 = 0.5$ and at 298 K.

up to about 1200 K in any of the three samples. Since no exotherm (around 923 K) due to the transformation of anatase to rutile is seen in the thermogram, we may conclude that no separate TiO_2 (like anatase) phase is present in samples A–C. The Ti–O–Si bond is quite stable to thermal treatment. The latter feature is reminiscent of TS-1 and titano-aluminosilicate-1 (9), which are also quite stable to thermal treatment up to 1200 K. Hence, even though MMATS samples lack the long-range order of TS-1, the Ti–O–Si bonds in both have similar characteristics at least with respect to thermal stability.

Framework IR and UV–VIS spectroscopy. The framework IR and UV–VIS spectra of these samples are shown in Figs. 7 and 8, respectively. The presence, in the IR spectra of samples A–C, of the 960 cm^{-1} band, probably due to a Si–O bond "perturbed" by Ti (20), is a further indication of the presence of Si–O–Ti linkages in MMATS. Both TS-1 and TS-2 exhibit this band and its intensity correlates with the content of Ti in their framework (21). The band at 550 cm^{-1} observed for TS-1 (Fig. 7) is due to the presence of five-membered rings (pentasil structure) in the crystalline material. This vibration is obviously not present in the amorphous titanosilicates. The UV spectra of MMATS (Fig. 8) is more complex. In addition to a strong absorption around 220 nm, which is characteristic of Ti^{4+} in tetrahedral symmetry, there is also significant absorption in the region 220–300 nm, suggesting that, compared to TS-1 (which has a sharp absorption band at 220 nm), the coordination of Ti^{4+} in MMATS is more heterogeneous. The Ti ions are most probably also present in other distorted tetrahedral/octahedral environments (see *Raman spectroscopy*). In these materials, Ti coordinates to four oxygen atoms, but because of its larger covalent radius, it can interact with one or two more ligands such as H_2O. This expands its coordination to a five or sixfold one. It is noteworthy that anatase (absorption at 330 nm) is not found in samples A–C (Fig. 8). To summarize, framework

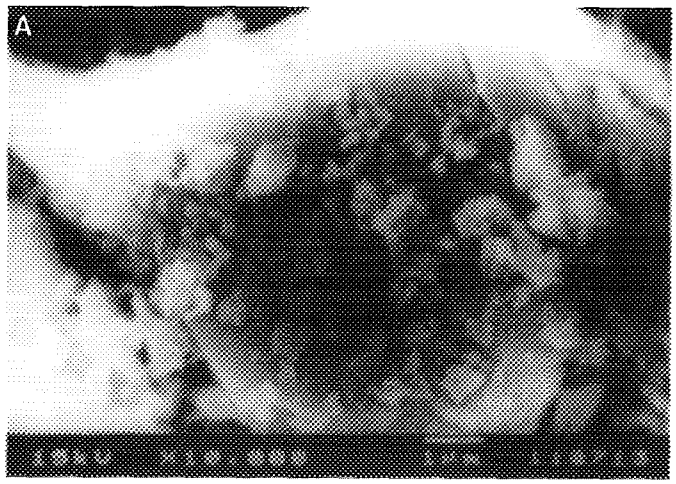

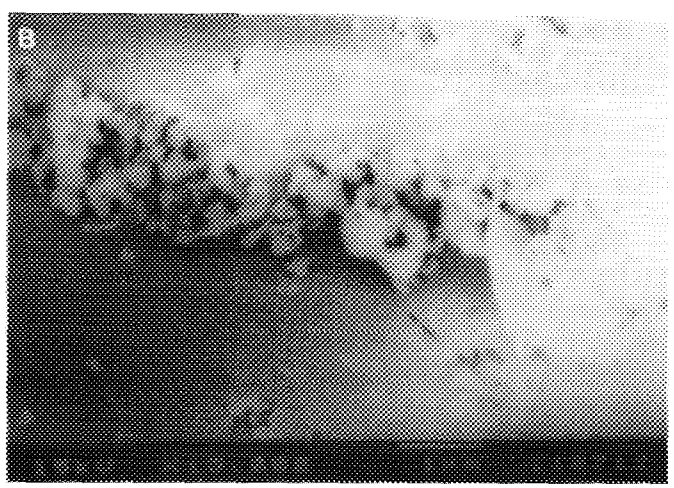

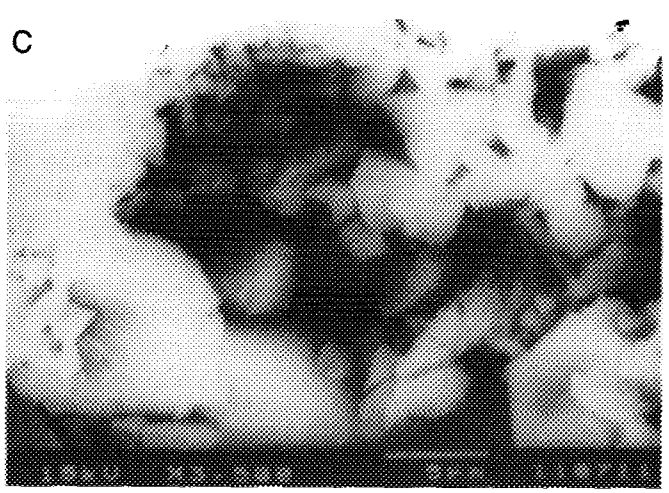

FIG. 5. Scanning electron micrographs of MMATS samples A, B, and C.

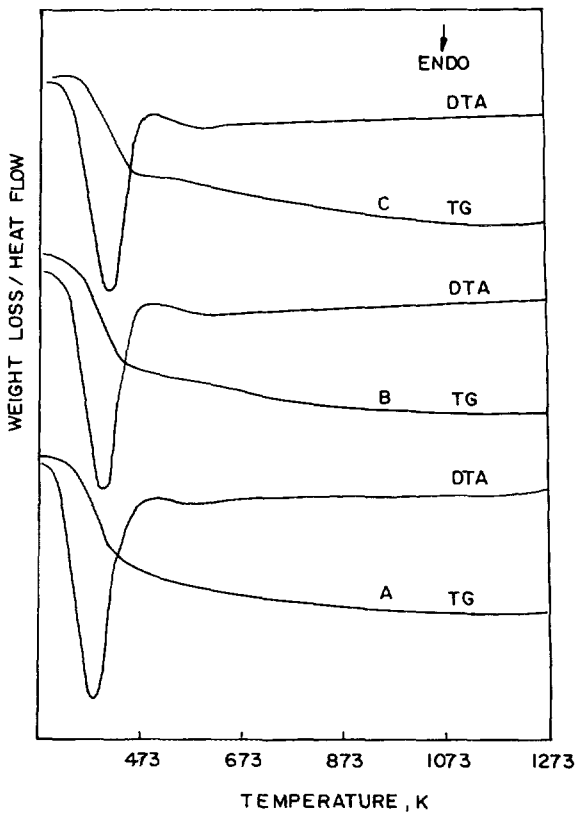

FIG. 6. Simultaneous TG–DTA thermograms of samples A, B, and C (curves A, B, and C, respectively).

IR and UV–VIS spectra indicate that (i) in MMATS samples SI–O–Ti linkages exist, (ii) the Ti^{4+} ions are present in tetrahedral (and probably also in octahedral) environments, and that (iii) a separate, crystalline TiO_2 phase, like anatase, is absent. However, the IR spectrum of MMATS differs from that of TS-1 with respect to the band at 550 cm^{-1} which is present in the latter case due to the presence of five membered rings.

Raman spectroscopy. The Raman spectra of samples A–C (curves a–c, respectively), a sample of SiO_2 prepared by the alkoxide method (curve d), and TiO_2 (anatase, curve e) are shown in Fig. 9. TiO_2 has strong bands at 640, 518, and 400 cm^{-1} as well as at 368, 248, and 146 cm^{-1} (not shown in Fig. 9). These values for anatase are similar to those observed by Deo *et al.* (22) (637, 513, 386, and 144 cm^{-1}) and Srinivasan *et al.* (23) (643, 520, 399, 244, and 144 cm^{-1}). From the presence of a broad band around 640 cm^{-1} and its increase with Ti content (Fig. 10), we may conclude that, even though a segregated, crystalline anatase phase may be absent, Ti^{4+} ions in a distorted octahedral symmetry are, probably, present in all our samples, A to C. Another feature of the spectra in Fig. 9 is the enhanced intensity of the Raman scattering in samples

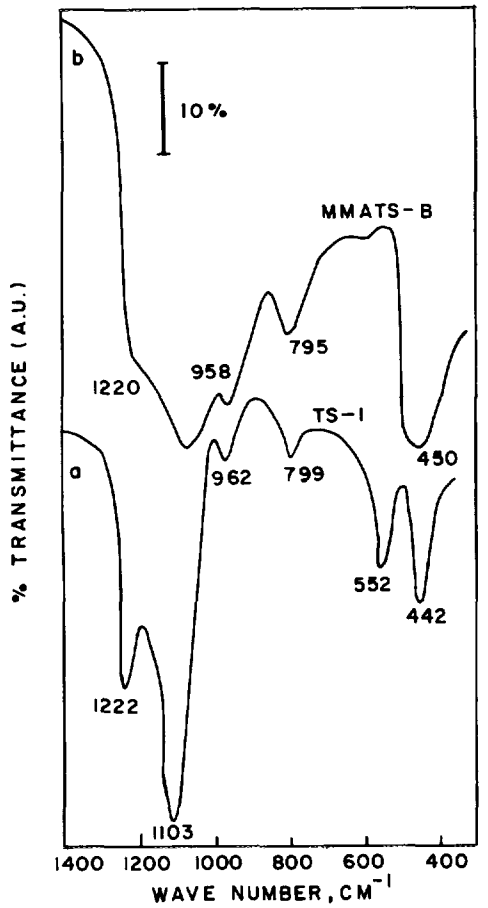

FIG. 7. FTIR spectra of crystalline TS-1 (curve a) and MMATS-B (curve b) samples.

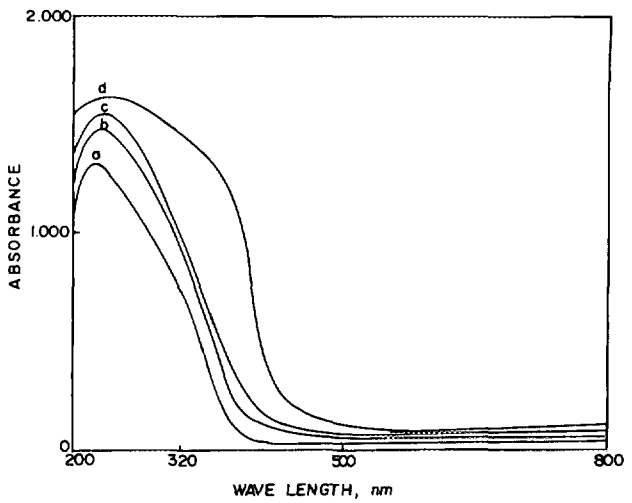

FIG. 8. UV–VIS spectra of MMATS samples A–C (curves a–c, respectively) and pure TiO_2 (curve d).

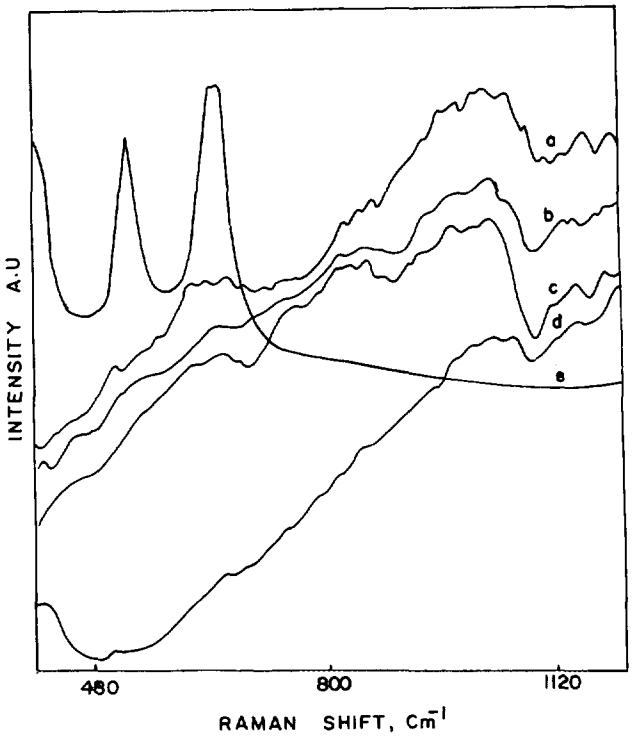

FIG. 9. Raman spectra of MMATS samples A–C (curves a–c respectively), pure SiO_2 (curve d), and pure TiO_2 (curve e).

A–C (compared to SiO_2, curved) around 800–850, 950–1000, and 1100–1150 cm^{-1}, respectively. Deo *et al.* (22), investigating the substitution of Ti in the crystalline silicalite-1 lattice, have also observed enhanced Raman scattering at 970 and 1125 cm^{-1} in TS-1 compared to silicalite-1 samples. While both these bands are essentially due to silicon–oxygen vibrations, the enhancement in their intensity is, perhaps, indicative of Si–O–Ti bond formation. All solid titania compounds exhibit Raman scattering below 900 cm^{-1} (22, 23).

^{29}Si MAS NMR spectroscopy. The structural connectivity of Ti to Si through Si–O–Ti bonds is again suggested by the ^{29}Si MAS NMR spectra (Fig. 10). The broadening of the ^{29}Si lines in samples A–C compared to those in pure SiO_2 (prepared by a similar procedure) suggests that species such as $Si(OSi)_{4-n}(OTi)_n$ exist in these samples resulting from the replacement of Si in $Si(OSi)_4$ by Ti in the second coordination sphere. In the completely homogeneous sol–gel method of preparation, as the miscibility of the precursors of silica and titania increases, the Ti–O–Si bond formation occurs more easily (8).

TPR. The stability of the Si–O–Ti bond in MMATS to reduction in H_2 by temperature-programmed reduction indicated that the Ti^{4+} ions are not reduced under flowing dry H_2, at least up to 1100 K. The nonreducibility of

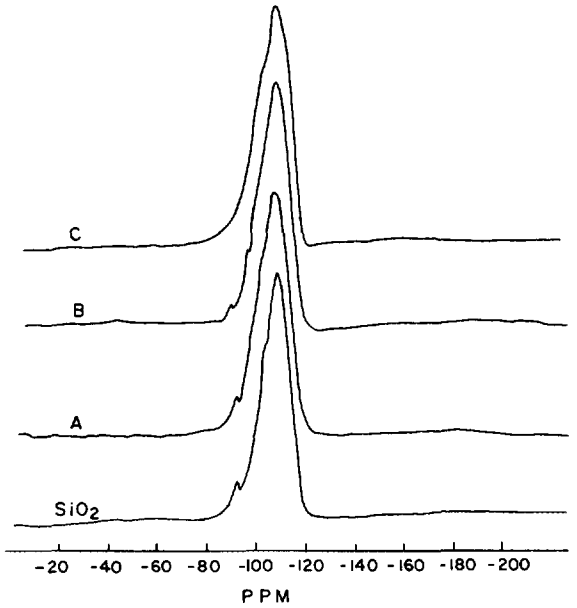

FIG. 10. ^{29}Si MAS NMR spectra of pure silica and MMATS samples A, B, and C.

MMATS under H_2 is probably due to the absence of a separate TiO_2 phase in them, and, in this respect, it is similar to TS-1.

X-ray scattering. The results from the characterization studies discussed above suggest that even though MMATS materials are amorphous and lack long-range order, there are broad similarities in the local environment around Ti^{4+} ions between them and titanosilicate molecular sieves, like TS-1. The local structural environment around Si and Ti in samples A–C was investigated using X-ray scattering techniques (10). The radial electron density distribution plots for a sample of SiO_2 prepared by the sol–gel method (see Experimental), samples A–C, and TiO_2 (anatase) are shown in Fig. 11. Values of interatomic distances derived from Fig. 11 are given in Table 3. The values for SiO_2 (1.63 (Si_1–O_1); 2.61 (O_1–O_1); 3.39 (Si_1–Si_2); and 4.24 Å (O_1–O_2)) are in the range usually observed for amorphous SiO_2 (24). The TiO_2 sample has the interatomic vectors at 1.99, 2.98, 3.93, and 4.74 Å, respectively. Two conclusions (of a qualitative nature) may be drawn from Fig. 11 on the effects of introduction of Ti in the silica matrix: (i) There is no evidence for the presence of anatase or an anatase-like phase in any of the amorphous titanosilicate samples MMATS, A–C. The r.e.d. curve for TiO_2 (anatase) is completely different from that of MMATS (Fig. 11); the peak at 2.98 Å, very significant in TiO_2, is absent in the MMATS samples. (ii) As the Ti content increases (from MMATS-C to MMATS-A), there is a gradual broadening of the peaks at 2.61 and 3.39 Å due to the O_1–O_1 and Si_1–Si_2 (Si_1–Ti_1), respectively. A plausible explanation for this observation is that the Ti atom is being inserted in the second coordination sphere of Si (oxygen atoms occupy the first coordination sphere) progressively in the series SiO_2 → MMATS-C → MMATS-B → MMATS-A. As expected, the introduction of Ti does not change the Si_1–O_1 distances significantly (Table 3). The statistical average of the Si_1–Si_2 and Si_1–Ti_1 vectors in the second coordination sphere varies from 3.29 to 3.40 Å. MMATS-C with the lowest content of Ti does not show any significant distortion in the Si_1–Si_2 vector. In MMATS-B and especially in MMATS-A, which contain higher amounts of Ti, the Si_1–Si_2 vector is shifted to lower values on introduction of Ti. Blasco *et al.* (25) have recently studied the local environment of Ti and Si in titano–aluminosilicates, isomorphous with zeolite beta, by the EXAFS technique and obtained a good fitting of the data for a model involving four silicon atoms in the second shell of Ti at a distance of about 3.23 Å implying the existence of isolated TiO_4 units. The shift (from 3.39 for SiO_2 to 3.29 Å for MMATS) observed in the peak due to Si_1–Si_2 distance in Fig. 11 can arise due to a contribution from a vector at 3.23 Å due to Si_1–Ti_1 from isolated TiO_4 tetrahedra present in the MMATS samples.

Catalytic Activity

The catalytic activity of MMATS in the oxidation (using aqueous H_2O_2 as oxidant) of benzene, toluene, and phenol was investigated (Tables 4 and 5). The amorphous titanosil-

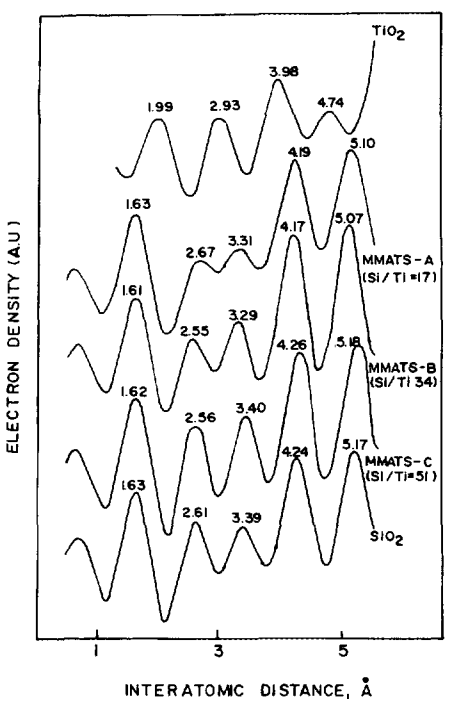

FIG. 11. Radial electron density distribution function curves for MMATS (A–C), SiO_2, and TiO_2 samples.

TABLE 3

Interatomic Distance Vectors in Silica, Titania and Titanosilicates

Sample	Si/Ti ratio	Interatomic vectors (Å)				
		Si_1–O_1	O_1–O_1	Si_1–Si_2 (Si_1–Ti_1)	O_1–O_2 (Si_1–O_2)	Si_1–Si_3 (O_1–O_3)
SiO_2	—	1.63	2.61	3.39	4.24	5.17
C	51	1.62	2.56	3.40	4.26	5.18
B	34	1.61	2.55	3.29	4.17	5.07
A	17	1.63	2.67	3.31	4.19	5.10
TiO_2	—	1.99 (Ti_1–O_1)	2.98 (O_1–O_1)	3.93 (Ti_1–Ti_2)	4.74 (Ti_1–O_2)	—

icates have significant catalytic activity in the oxidation of benzene (to phenol) and phenol (to hydroquinone and catechol). Both pure TiO_2 and Ti-impregnated silica were found to have negligible activity in these reactions. Hence, the catalytic activity must be due to isolated TiO_4 species present in MMATS samples. The course of the hydroxylation of phenol on the three samples is shown in Fig. 12. The reaction occurs with an induction period and catechol is the first dihydroxybenzene obtained. However, *para*-benzoquinone is formed as soon as the reaction starts. A large concentration of H_2O_2 in the beginning of the reaction probably leads to a fast overoxidation of hydroquinone in the reaction medium. From the initial rates, the intrinsic activity of TS-1 appears to be high (Table 4). However, under the conditions given in Table 4 (phenol/H_2O_2 (mol) = 3), the H_2O_2 efficiencies for TS-1 and MMATS-A are found to be 91 and 93%, respectively, at the end of the reaction. A lower H_2O_2 efficiency observed for samples B and C is due to their lower concentration of isolated Ti species which are probably covered with tar during the initial stages of the reaction. In the absence of fresh Ti surface, the self-decomposition of H_2O_2 is predominant and hence the efficiency of utilization of H_2O_2 in the hydroxylation of phenol is low. The main difference between TS-1 and MMATS-A lies in the product distribution. Due to the mesoporous nature of the material, no shape selectivity is seen for the latter. In the oxidation of phenol, for example, the ratio of the *ortho*- to the *para*-isomer (catechol/hydroquinone) is around 2 using the MMATS-A sample, in contrast to the TS-1 catalyzed oxidation where a value of around 1 or even less than 1 is observed due to the shape selectivity of the medium pores in the titanosilicate molecular sieve (Table 4) (26).

The catalytic activity and the product distribution in the oxidation of benzene and toluene over sample A (Si/Ti = 17) are summarized in Table 5. In the oxidation of benzene, the selectivity to phenol is almost 100% at a conversion of 13.3 mol% of benzene (benzene/H_2O_2 (mol) = 3). The

TABLE 4

Hydroxylation of Phenol over Amorphous Titanosilicate (MMATS) Samples[a]

Sample	Turn over frequency[b]	H_2O_2 efficiency (%)[c]	Product distribution (wt%)	
			Catechol	Hydro- and *p*-benzoquinones
A	2.5	93.0	63.2	36.8
B	1.6	31.5	71.4	28.6
C	1.2	26.4	90.0	10.0
TS-1	5.5	91.2	47.5	52.5
TiO_2	negligible	—	—	—
SiO_2	no activity	—	—	—
Ti impreg SiO_2	no activity	—	—	—

[a] Catalyst: A–C (Si/Ti = 17, 34, and 51, respectively); Temperature: 353 K; Phenol/catalyst (wt) = 10; Phenol/H_2O_2 (mol): 3; Solvent (water): 20 g. Duration = 18 h.

[b] Initial rates, moles converted per hour per Ti atom.

[c] Moles of H_2O_2 consumed in the formation of dihydroxy benzenes excluding tar.

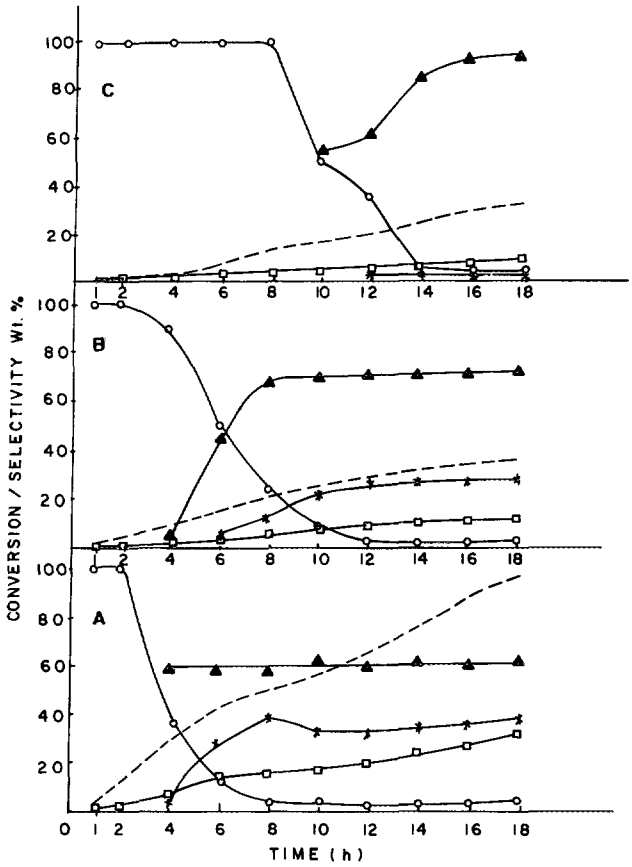

FIG. 12. Conversion (mol%) and selectivity (%) to different products in the hydroxylation of phenol over MMATS samples A to C as a function of time. (□) Phenol conversion; (▲) Catechol; (*) Hydroquinone; (○) Parabenzoquinone; (---) H_2O_2 efficiency (mol%). (Conditions are as given in Table 4)

H_2O_2 efficiency is 40%. The latter value is lower on the other two mesoporous titanium silicates, viz., Ti–HMS and Ti–MCM—41 in the oxidation of benzene (5). A conversion of only 37 and 68%, respectively, has been observed even at a ninefold higher concentration of H_2O_2 (benzene/H_2O_2 = 0.35). In the oxidation of toluene, a surprising observation in Table 5 is the formation of products due to the oxidation of the side chain (methyl group) of toluene (benzyl alcohol, benzaldehyde, and benzoic acid) in addition to the formation of cresols. In fact, oxidation of the methyl substituent in toluene is more predominant (69% product selectivity) than aromatic hydroxylation (31%). Such a phenomenon, while common in the case of vanadosilicates, VS-2 and V-NCL-1 (27, 28), has so far not been observed over titanosilicates TS-1 or TS-2. The latter selectively produce only cresols in the oxidation of toluene (29). The mechanism of oxyfunctionalization of the organic substrates over MMATS is, hence, different from that over TS-1 or TS-2, and probably involves free radical routes. The ability of our amorphous titanosilicates to utilize aqueous H_2O_2 in oxidation reaction is additional evidence for the presence of Ti^{4+} ions in tetrahedral coordination in the silicate matrix.

SUMMARY AND CONCLUSIONS

Novel, amorphous titanosilicates with a bimodal, fairly narrow pore size distribution with average pore widths around 0.85 and 3.6 nm, respectively, have been synthesized from the corresponding alkoxides at neutral pH in the absence of nitrogenated organic bases, acids, or other bases. The Ti^{4+} ions are well dispersed in these materials, forming Ti–O–Si bonds. There is no evidence for the presence of a separate TiO_2 phase. TG/DTA analysis and temperature-programmed reduction in H_2 indicate that these Ti atoms do not migrate and sinter to form TiO_2 at elevated temperatures nor are they reduced easily to lower oxidation states in H_2. X-ray scattering studies suggest that at least a part of the Ti atoms are in a tetrahedral environment of oxygen atoms. These titanosilicates are active in oxidation reactions using aqueous H_2O_2 as the oxidizing agent. In some cases, as in the oxidation of phenol to catechol and hydroquinone, their activity and selectivity is comparable to the titanium-molecular sieve, TS-1, or the new mesoporous materials like Ti-HMS and Ti-MCM-41. MMATS is unique among the solid catalysts investigated so far in yielding more catechol than hydroquinone in the oxidation of phenol by H_2O_2. The oxyfunctionalization of the methyl substituent in toluene to give benzyl alcohol, benzaldehyde, and benzoic acid in addition to cresols distinguishes MMATS from TS-1 or TS-2.

TABLE 5

Catalytic Activity of Amorphous Titanosilicate (MMATS) in the Oxidation of Benzene and Toluene[a]

Substrate	Solvent	Substrate conv. (mol%)	H_2O_2 efficiency (mol%)[b]	Product distribution (wt%)
Benzene	acetone	13.3	40	Phenol: 100
Toluene	acetonitrile	26.6	39	benzyl alcohol: 16.0 benzaldehyde: 49.1 benzoic acid: 3.9 *o*-cresol: 14.0 *p*-cresol: 16.5 others: 0.5

[a] Catalyst sample: A (Si/Ti = 17); Temperature: 353 K; Substrate/Catalyst (wt) = 10; Substrate/H_2O_2 (mol): 3 (for benzene) and 1 (for toluene); Solvent: 20 g; duration = 18 h.

[b] H_2O_2 efficiency based on utilization of H_2O_2 for the formation of all oxidized products.

ACKNOWLEDGMENTS

A. Keshavaraja thanks CSIR, New Delhi for a research fellowship. The authors are grateful to Dr. S. Badrinarayanan for XPS and Dr. S. T. Kshirasagar for Raman spectral measurements.

REFERENCES

1. Taramaso, M., Perego, G., and Notari, B., US Patent 4,410,50 (1983); Notari, B., *Stud. Surf. Sci. Catal.* **60,** 343 (1991).
2. Reddy, J. S., Kumar, R., and Ratnasamy, P., *Appl. Catal.* **58,** L1, (1990).
3. Serrano, D. P., Li Hong-Xin, and Davis, M. E., *J. Chem. Soc., Chem. Commun.* 745 (1992).
4. Camblor, M. A., Corma, A., Martinez, A., and Perez-Parient, J., *J. Chem. Soc., Chem. Commun.* 8 (1992); Camblor, M. A., Corma, A., and Perez-Pariente, J., *Zeolites* **13,** 82 (1993).
5. Tanev, P. T., Chibwe, M., and Pinnavaia, T. J., *Nature* **368,** 321 (1994).
6. Corma, A., Navarro, M. T., Perez-Pariente, J., and Sanchez, F., *J. Chem. Soc., Chem. Commun.* 147 (1994); *Stud. Surf. Sci. Catal.* **84,** 69 (1994).
7. Franke, O., Rathonsky, J., Schulz-Ekloff, G., Starek, J., and Zukal, A., *Stud. Surf. Sci. Catal.* **84,** 77 (1994).
8. Toba, M., Mizukami, F., Niwa, S., Sano, T., Maeda, K., Annila, A., and Komppa, V., *J. Mol. Catal.* **91,** 277 (1994).
9. Thangaraj, A., Kumar, R., Mirajkar, S. P., and Ratnasamy, P., *J. Catal.* **130,** 1 (1991).
10. Ratnasamy, P., and Leonard, A. J., *Catal. Rev.* **6,** 293 (1972).
11. Horvath, G., and Kawazoe, K., *J. Chem. Eng. Jpn.* **16,** 470 (1983).
12. Barrett, E. P., Joyner, L. G., and Halenda, P. H., *J. Am. Chem. Soc.* **73,** 373 (1951).
13. Ramesh Reddy, K., Ramaswamy, A. V., and Ratnasamy, P., *J. Catal.* **143,** 275 (1993).
14. Imamura, S., Ishida, S., Tarumoto, H., and Saito, Y., *J. Chem. Soc., Faraday Trans.* **89,** 757 (1993).
15. Saito, Y., *J. Phys. Soc. Jpn.* **53,** 4230 (1984).
16. Mukhopadhyay, S. M., and Garofalini, S. H., *J. Non-Cryst. Solids* **126,** 202 (1990).
17. Rosenthal, A. B., and Garofalini, S. H., *J. Non-Cryst. Solids* **107,** 65 (1988).
18. Kusabaraki, K., *J. Non-Cryst. Solids* **95, 96,** 411 (1987).
19. Hanase, T., Aikawa, T., and Saga, N., *J. Am. Cearm. Soc.* **67,** 52 (1984).
20. Boccuti, A. R., Rao, K. M., Zecchina, A., and Leofanti, G., *Stud. Surf. Sci. Catal.* **48,** 133 (1988).
21. Huybrechts, D. R. C., Buskans, P. L., and Jacobs, P. A., *J. Mol. Catal.* **71,** 129 (1992).
22. Deo, G., Turek, A. M., Wachs, I. E., Huybrechts, D. R. C., and Jacobs, P. A., *Zeolites* **13,** 365 (1993).
23. Srinivasan, S., Datye, A. K., Hampden-Smith, M., Wachs, I. E., Deo, G., Jehng, J. M., Turek, A. M., and Peden, C. H. F., *J. Catal.* **131,** 260 (1991).
24. Fripiat, J. J., Leonard, A., and Barake, N., *Bull. Soc. Chem. France* 122 (1963).
25. Blasco, T., Camblor, M. A., Corma, A., and Perez-Pariente, J., *J. Am. Chem. Soc.* **115,** 11806 (1993).
26. Thangaraj, A., Kumar, R., and Ratnasamy, P., *J. Catal.* **131,** 294 (1991).
27. Hari Prasad Rao, P. R., Belhekar, A. A., Hegde, S. G., Ramaswamy, A. V., and Ratnasamy, P., *J. Catal.* **141,** 595 (1993).
28. Hari Prasad Rao, P. R., Ramesh Reddy, K., Ramaswamy, A. V., and Ratnasamy, P., *Stud. Surf. Sci. Catal.* **78,** 385 (1993).
29. Ramaswamy, A. V., Sivasanker, S. and Ratnasamy, P., *Microporous Mater.* **2,** 451 (1994).